

Mirae Kim · Hamid Reza Karbasian · Eunseop Yeom 

# Transient three-dimensional flow structures of oblique jet impingement on a circular cylinder

Received: 27 November 2017 / Accepted: 3 December 2017 / Published online: 14 December 2017  
© The Visualization Society of Japan 2017

**Abstract** A large eddy simulation (LES) was conducted to visualize the three-dimensional (3D) flow structures of a round jet impinging onto a circular cylinder with an inclination angle of  $45^\circ$ . The Reynolds number of the round jet is 11,800, and the distance from the nozzle exit to cylinder surface is four times the jet diameter. To verify the LES results, planar particle image velocimetry (PIV) measurements were obtained using the same flow conditions. After the impingement, the jet becomes a 3D curved wall jet and is attached to the cylinder wall far downstream due to the Coanda effect. The time-averaged pressure field indicates that the jet attachment is caused by the strong suction pressure after the impingement. However, the instantaneous pressure field reveals that positive and negative pressure bands repeatedly appear with 3D vortex structures near the impinging point. Ring-like rollup structures expand in the circumference direction over time, and weakened vortices are sustained longer in the limited spanwise boundary. The most notable feature is that a clockwise rotational vortex moves down to the wall when the counter-clockwise rotational vortex moves up from the surface, followed by a sign change of the instantaneous wall pressure. The ensemble-averaged velocity fields show good agreement between the LES and PIV results.

**Keywords** Impinging jet · 3D flow structure · Cylinder · LES · PIV · Visualization

## 1 Introduction

Jet impingement has long been used as a direct and efficient way to transfer heat to solid surfaces and or remove heat from the solid surfaces. It has been observed many applications using the jet impingement, such as cooling hot surfaces, drying surfaces, chemical vapor deposition, VSTOL aircraft, booster rockets, cooling combustor walls and steam generator walls, glass and metal sheet manufacturing, cooling electronic components, aircraft de-icing, and cooling gas turbine blades. In particular, the flow structures resulting from jet impingement of surfaces were investigated by many researchers.

Earlier studies examined the flow structures and behavior resulting from jet impingement on flat surfaces (Donaldson and Snedeker 1971; Didden and Ho 1985; Landreth and Adrian 1990). These and other studies have established that a circular jet impinging on a flat surface perpendicularly can be divided into three distinct regions: a free-jet region, a stagnation region, and a wall-jet region. These regions result from the fact that after the free jet impinges on the flat surface, it essentially turns perpendicularly and moves radially away from the stagnation point along the flat surface. Jambunathan et al. (1992), Viskanta (1993), and Martin (1977) provide comprehensive reviews of studies on impinging jets. Such studies report on the effects of changing parameters such as the Reynolds number, nozzle-to-surface distance, nozzle geometry,

jet temperature and orientation, and the number of jets on the resulting flow and surface heat transfer. These studies also reported the effects on the flow field of different jet configurations, such as single round nozzle or slot nozzle and arrays of such nozzles.

However, less attention has been given to circular jet impingements on other types of surface geometries, particularly curved surfaces. Brahma et al. (1991) measured the static pressure and velocity profile of a slot jet impinging on a cylindrical surface. Chan et al. (2003) reported detailed turbulence data for various conditions of a slot jet impinging on a semi-circular cylinder. Wygnanski's research group studied wall jets on a gradually curving in an experiment to obtain the various flow characteristics. They analyzed the vorticity contours using particle image velocimetry (PIV) measurements and compared between plane and curved wall jets using the streamwise vortices (Neuendorf and Wygnanski 1999; Neuendorf et al. 2004; Han et al. 2006). Danon et al. (2016) measured the unsteady surface pressures using pressure-sensitive paint for a transient 2D wall jet over a circular cylinder.

Many applications involve flows impinging on surfaces that are not flat, such as NOTAR (NO Tail Rotor) helicopter (Cîrciu and Boşcoianu 2010), cast-in turbine airfoils (Terzis et al. 2014), turbine flow meter (Ali et al. 2016), and so on. Thus, this work examines the flow field characteristics of a round jet impinging on a convex surface in comparison to a slit jet. A flow field presents a unique flow geometry where an axisymmetric jet becomes a three-dimensional flow over the surface. The flow field around a cylinder with a round jet impinging on it tends to separate, and the Coanda effect makes the jet adhere to the surface. The adverse pressure gradient and the Coanda effect depend on the magnitude and turbulent intensity of the approaching jet velocity profile.

There are previous studies on a single round jet impinging on a cylindrical convex surface. Kornblum and Goldstein (1997) used a flow visualization technique to study round jets impinging onto convex and concave semi-cylindrical surfaces with low relative curvatures. A substantial amount of flow recirculation into the main jet flow was observed from the flow impinging on the surfaces. Cornaro et al. (1999) used a smoke wire technique for flow visualization of a round jet impinging on convex and concave surfaces. They also measured the local radial distributions of the axial velocity and turbulence intensity near the jet exit and along the jet centerline using the hot wire technique. Their flow visualization images show the initiation and breakdown of ring vortices as a function of the distance between the jet exit and the convex surface. These results support the similar research by Kornblum and Goldstein (1997).

Fleischer et al. (2001) used similar flow visualization methods to study the flow of a round jet impinging on a convex surface with the same experimental parameters. They found that there were two types of vortex breakup: one due to merging prior to impingement and another due to flow separation from the surface. Lee et al. (1997) investigated the flow properties and Nusselt number distribution of a round jet impinging on a curved surface using liquid crystal. Recently, Yi et al. (2016) investigated the heat transfer characteristics and quantitative visualizations of an oblique round jet impinging onto a high-temperature plate with different impingement angles and distances between the jet and the plane surface.

Esirgemez et al. (2007) provided more comprehensive information about the mean flow field characteristics for a circular jet ( $Re = 25,000$ ) impinging on a convex cylinder ( $D/d = 4$ ) at a separation distance of four jet diameters. The study was conducted using a laser Doppler anemometry technique. Their results demonstrated that a circular free jet becomes highly three-dimensional after impinging on a convex cylinder and wrapping around it. Unfortunately, little detailed information on the latter flow mechanism was provided. New and Long (2015) observed the 3D flow and vortex structure dynamics of a round jet impinging on a circular cylinder. However, their study examined laminar flow, and three-dimensional studies of turbulence are needed, considering that turbulence is more common than laminar flow.

Recently, we have confirmed that most of the fluid moves in one direction when  $45^\circ$  oblique impingement (Kim et al. 2017). Compared to normal impingement, there are interesting phenomena such as Coanda effect and flow separation delay. However, this study is measured by planar PIV along the centerline of the jet, so it is necessary to investigate 3D flow structures of oblique impingement. Therefore, the present study sheds more light on the detailed 3D flow structures of a round jet impinging obliquely on a convex circular cylinder. This was accomplished using large eddy simulation (LES) and PIV measurements. To the best of our knowledge, such a study has not been reported previously for a 3D curved wall jet over a circular cylinder. Special attention was given to the evolution of the vortex structures after the impinging jet reorients itself along the cylindrical surfaces and the resulting instantaneous wall pressure distributions. The flow interpretations were compared to slit jet impingement on a circular cylinder. Finally, the LES results were validated by comparison with velocity field measurements using PIV.

## 2 Methods

### 2.1 Numerical method

An impinging jet over a circular cylinder was numerically investigated using computational fluid dynamics (CFD). The Navier–Stokes equations were discretized by the finite-volume method (FVM). The flow structure over the cylinder was solved using the LES approach with a WALE sub-grid model. A computational domain with a structured mesh was designed with  $1.8 \times 10^6$  cells. The first grid distance from the wall is  $1.5 \times 10^{-5} D$  to obtain  $y^+$  lower than 1. Figure 1 shows the structured mesh around a circular cylinder.

To increase the quality of the simulations, a boundary layer mesh was established around the wall surface of the cylinder. No-slip conditions are applied to the wall surface of the cylinder, and the outer boundaries have outlet conditions with atmospheric pressure. The jet velocity in the nozzle is set as an inlet velocity with uniform flow. The turbulence intensity measured by PIV at the inlet of the nozzle is 22%. Hence, this value was also added to the inlet velocity to have the same conditions as the experimental case. The bounded central differencing scheme was used for spatial discretization, and the SIMPLEC method was applied for pressure–velocity coupling. For temporal formulation, the second-order implicit scheme was selected to obtain higher resolution. The CFD flow solver package ANSYS Fluent version 16.1 (ANSYS Fluent, Academic Research, V16.1 2015) was used for the modeling.

Different time steps were examined, and  $\Delta t = 1.5 \times 10^{-6} T$  led to a Courant–Friedrichs–Lewy (CFL) number lower than 2. Domains with different numbers of nodes (coarse, fine, and very fine grids) were examined, and the time-averaged velocity profiles were computed for when the flow reaches steady state for each case. The results showed that errors of 10.08 and 0.13% were obtained for the respective velocity profile deviations resulting from coarse and fine meshes compared to the very fine mesh (Table 1). Therefore, the fine mesh was used for the investigations.

### 2.2 Experimental method

Figure 2 shows the experimental setup of the conventional PIV system used for the velocity field measurements. The flow characteristics were characterized based on the Reynolds number ( $Re\#$ ), cylinder diameter ( $D$ ), jet nozzle diameter ( $d$ ), and distance between the jet nozzle and cylinder surface ( $H$ ). An aluminum cylinder with a diameter of 50 mm was anodized to prevent light scattering. A jet nozzle with an inner diameter of 3 mm was connected to an air compressor. The distance from the nozzle to the cylinder surface was fixed such that  $H/d$  was equal to 4.

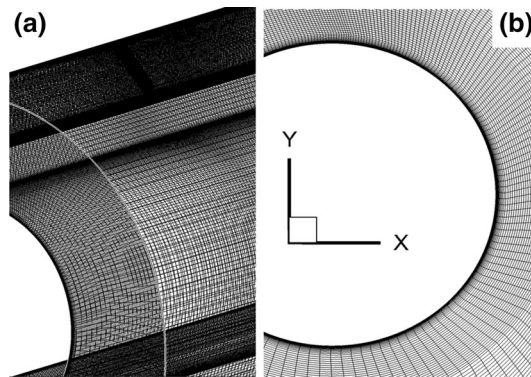


**Fig. 1** Structured mesh around a circular cylinder

**Table 1** Errors for deviation of time-averaged velocity profile for grid conditions

Domain	Number of cells	Errors for time-averaged velocity profile
Coarse	$1 \times 10^6$	10.08%
Fine	$1.8 \times 10^6$	0.13%
Very fine	$3.2 \times 10^6$	–

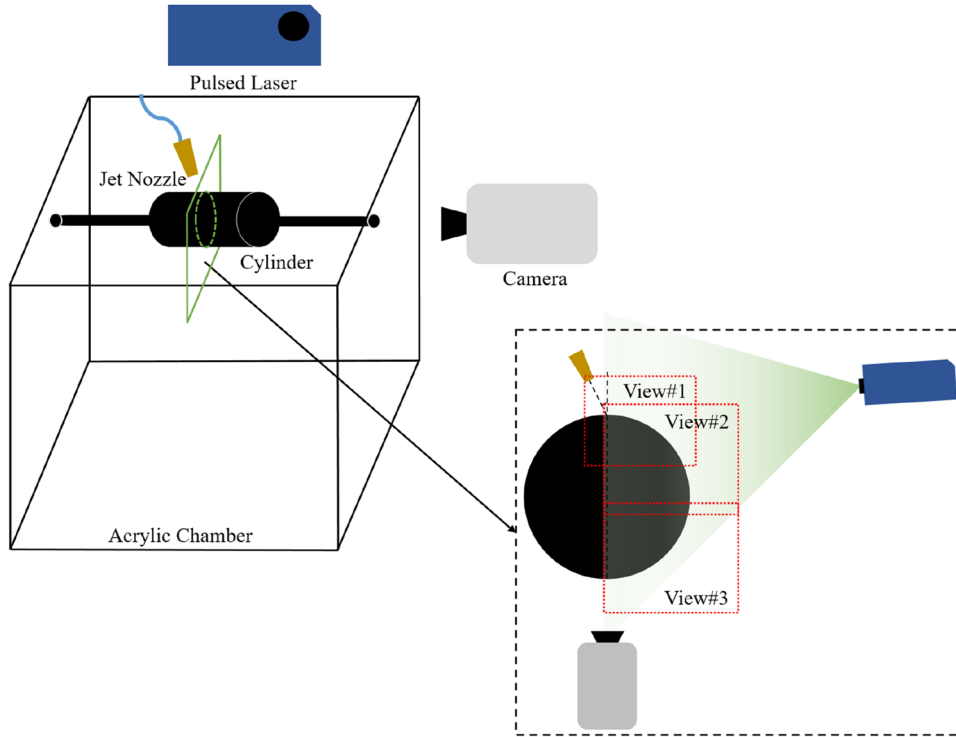


**Fig. 2** Experimental setup and field of view for PIV measurements

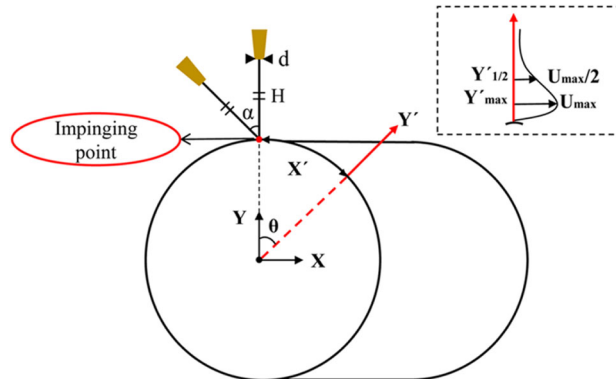


**Fig. 3** Flow configuration and coordinate system of the mean velocity profile

The impingement angle ( $\alpha$ ) is the angle between the jet axis and the direction normal to the circular cylinder surface (see Fig. 3). The Reynolds number was defined as  $(4Q/\pi d^2) \cdot d/\nu$ , where  $Q$  is the volumetric flow rate of the jet, and  $\nu$  is the kinematic viscosity. A Reynolds number of 11,800 and nozzle angle of  $45^\circ$  were selected to investigate the three-dimensional flow structures. The whole field of view for the PIV measurement includes the curved wall jet area over half of the cylinder in the direction normal to the wall, including the impingement area. Due to the limitations of each view, different fields of view were reconstructed by merging two subsections (view #2 and view #3 in Fig. 2) without the impingement area (view #1 in Fig. 2) for the analysis of the whole field of view. For each section, the PIV parameters such as the time interval were varied to optimize the PIV measurement according to the 1/4 rule (Keane and Adrian 1992).

Illumination was applied using a Nd:Yag pulse laser (New Wave, Gemini PIV, USA) with around 200 mJ per pulse and a wavelength of 532 nm. A CCD camera was connected with a 120-mm lens (Canon 120 mm f/2.8) for view #1, and a 60-mm lens (Canon 60 mm f/2.8) was used for view #2, and view #3 to obtain a particle image. The image resolution was 0.0256 mm/pixel for view #1, and 0.0333 mm/pixel for view #2 and view #3. An olive oil aerosol generated by a Laskin nozzle was used as tracer particles with

diameters of  $2 \pm 1 \mu\text{m}$ . These particles have an adequate aerodynamic response to velocity gradients in turbulent or gas flows (Melling 1997). The selected field of view with this optical setup provides a particle image diameter of 3–4 pixels, and the image plane is well focused to reduce uncertainty. An acrylic chamber with dimensions of  $500 \text{ mm} \times 500 \text{ mm} \times 450 \text{ mm}$  was used to produce the optimal amount of oil particles. The size of the chamber was much larger than the computational domain, so it did not affect the flow.

Velocity vectors were obtained using a two-frame cross-correlation method. The size of the interrogation window was  $32 \times 32$  pixels, and 50% overlap was allowed. An in-house post-processing program (PIVACE) with a two-frame cross-correlation method was used to remove error vectors. The program includes a sub-pixel searching algorithm that uses a Gaussian fitting function for velocity interrogation. Error vectors were removed by a median filter and replaced with new vectors obtained using an interpolation method. To avoid circular correlation, the second frame was made two times bigger than the first frame. The ensemble-averaged velocity field was obtained using 1000 PIV measurements.

### 2.3 Validation of LES results

To validate the numerical results, the mean velocity contours and profiles obtained by PIV experiments were compared with those from the LES results. Figure 3 shows a schematic of the flow configuration and the coordinate system of the curved wall jet. To obtain the mean streamwise velocity component ( $U$ ) distribution over the curved wall jet, the radial coordinate  $Y'$  ( $= \sqrt{X^2 + Y^2} - R$ ) is required, which is normal to the curved surface and originates from the center of the cylinder. The velocity vectors were recalculated according to the  $Y'$  direction. The maximum streamwise velocity  $U_{\text{max}}$  occurs at the radial location  $Y'_{\text{max}}$ .  $Y'$  was normalized using the jet's half-width  $Y'_{1/2}$ , which is the distance from the surface to the point where the velocity magnitude is half of the maximum mean streamwise velocity ( $U_{\text{max}}/2$ ). The cylindrical angle  $\theta$  originating from the impinging point was selected to compare the streamwise mean velocity profiles in the developing curved wall jet. The arc distance  $X'$  ( $= R\theta$ ) was calculated at each selected  $\theta$  and normalized by the nozzle diameter.

## 3 Results and discussion

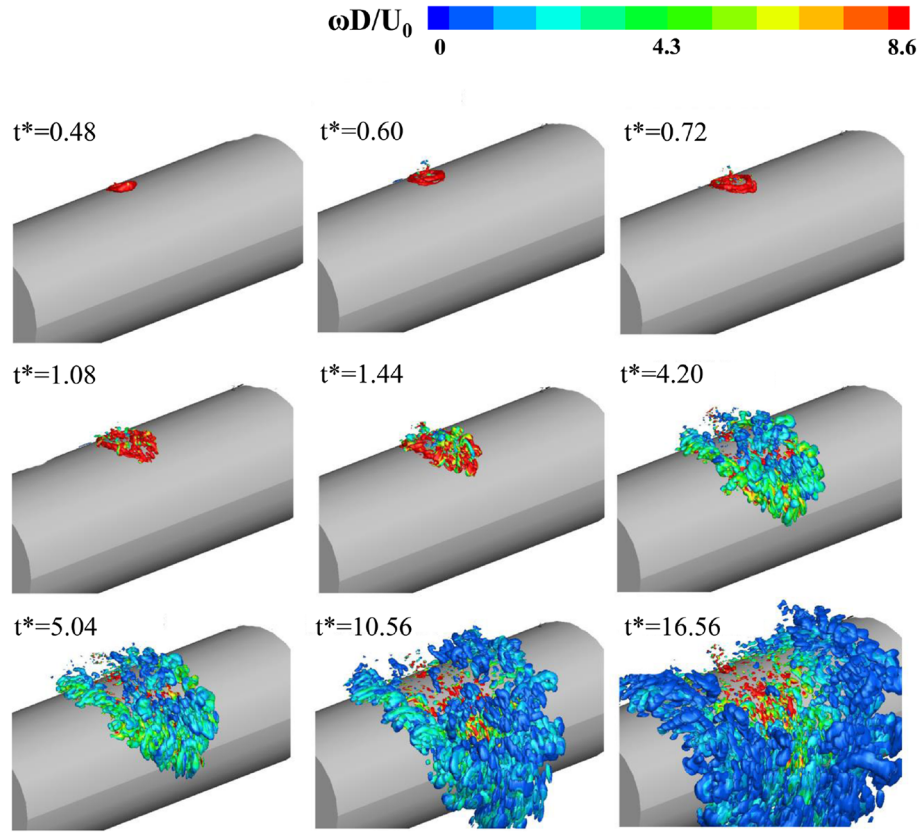
### 3.1 Evolution of 3D flow structures

Figure 4 shows the evolution of instantaneous 3D vorticity fields over time after impingement. The vortex structures are represented by the iso-contours of the second invariant of the velocity gradient tensor  $Q$  (Jeong and Hussain 1995). This physical quantity gives an indicator of the 3D flow structures where the deformation is dominated by the rotational movement along the cylinder surface. A non-dimensional form of the vorticity magnitude is provided. In the case of the vorticity magnitude,  $\omega$ ,  $D$ , and  $U_0$  are the vorticity, cylinder diameter, and jet velocity, respectively. Red denotes a positive value of vorticity with counter-clockwise rotations, while blue represents a negative value with clockwise rotations. The non-dimensional time  $t^*$  is defined as  $(4Q/\pi d^2) \cdot t/D$ , which is normal time divided by the convective time scale.

At the initial stage until  $t^* = 1.0$ , the round jet collides with the cylinder surface and ring vortices are formed along the jet shear layer. Two conjugate vortices are created in the flow field at  $t^* = 0.6$ . The ring vortices are elongated in the streamwise direction at  $t^* = 0.72$ . The vortices in the region of the impinging point originate from the turbulent round jet before impingement. Vortex structures quickly become turbulent after  $t^* > 1.0$ . The ring vortices break down and divide into smaller eddies due to the circumferential instability at  $t^* = 1.08$ . This unsteadiness leads to the appearance of small structures as the eddies lose their strength and distribute through tilting and stretching.

At  $t^* = 1.44$ , the 3D turbulent wall jet moves further in both the streamwise and spanwise directions. Unlike in flat-surface jet impingement, the core size of the ring vortex does not remain relatively invariant, regardless of the viewing orientation. In this case, the core size is drastically reduced shortly after it impinges on the wall, turns, and moves along the wall radially. Hairpin vortices are formed by the pairing of opposite-signed vortices. Negative values of vortices (clockwise rotation) are observed in the upper region of the attached wall jet. These vortices are generated from the wall due to the no-slip condition and viscosity.

At the stage of wall-jet development ( $t^* = 4.2$  and  $5.04$ ), the attached jet moves rapidly in the streamwise direction rather than the spanwise direction. The vortex structures are similar in the two cases.



**Fig. 4** Evolution of vortex structures over the circular cylinder after an oblique round jet impinges onto a cylinder

Small and strong positive vortices (red dots) are observed near the cylinder wall, while bigger negative vortices appear in the upper region of the wall jet. These negative vortex structures seem to align with the streamwise direction. Weak, large, hairpin, or cane-like structures are observed along the jet edge formed by the vortex pairing process.

At  $t^* = 10.56$ , the 3D curved wall jet starts to separate from the circular cylinder and enters steady state at  $t^* = 16.56$ . Strong positive vortices are observed near the cylinder surface, and strong negative vortices are located in the upper region of the wall jet. Both positive and negative vortices seem to align with the streamwise direction at  $t^* = 10.56$ . When the 3D curved wall jet is fully developed ( $t^* > 15$ ), no further extension of the jet into the spanwise direction is observed. It can be concluded that the spanwise extension of the jet is limited to  $\pm 1D$  from the impinging point in this flow configuration.

The strong shear layer near the impingement area makes some small-scale vortices with high vorticity. These structures distribute throughout the surface and break down into multiple structures with lower vorticity. Interestingly, large-scale negative vortex structures move away from the wall jet and sustain longer along the edge of the wall jet. This is because of the buoyancy effect which occurred by centrifugal force generated by the curvature. Unlike a 2D curved wall jet along a circular cylinder wall (Neuendorf et al. 2004; Danon et al. 2016), streamwise vortex structures cannot be found in the 3D curved wall jet.

Figure 5 shows the surface pressure distributions at the cylinder wall when the 3D wall jet reaches steady state. Figure 5a shows an instantaneous wall pressure field, and Fig. 5b shows the time-averaged pressure field on the cylinder wall. Both figures show a distinct circle indicating a region of positive pressure because of the round jet impingement. However, a strong negative (suction) pressure region appeared due to the Coanda effect. The suction pressure distribution has been measured in the previous research (Brahma et al. 1991; Danon et al. 2016) for the case of a 2D slit curved wall jet on a circular cylinder. However, there is no previous report on the wall pressure field associated with a round jet impingement on a circular cylinder.

Because of the suction pressure on the cylinder surface, the 3D curved wall jet attaches to the wall longer than a uniform flow past a circular cylinder. The most interesting aspect is that the pressure in the impingement area is not always negative in the instantaneous pressure distribution (Fig. 5a). This is the first

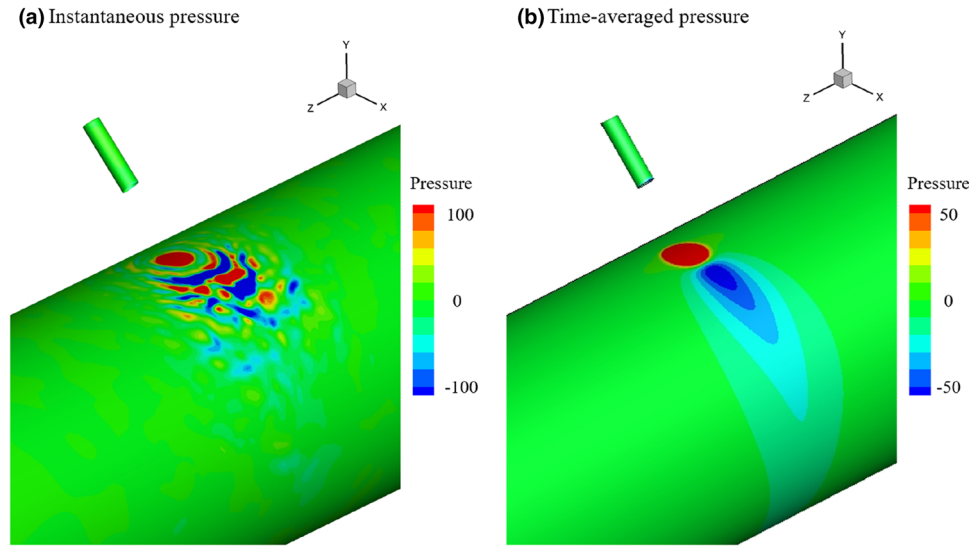


**Fig. 5** Instantaneous and time-averaged wall pressure fields on the surface of a circular cylinder

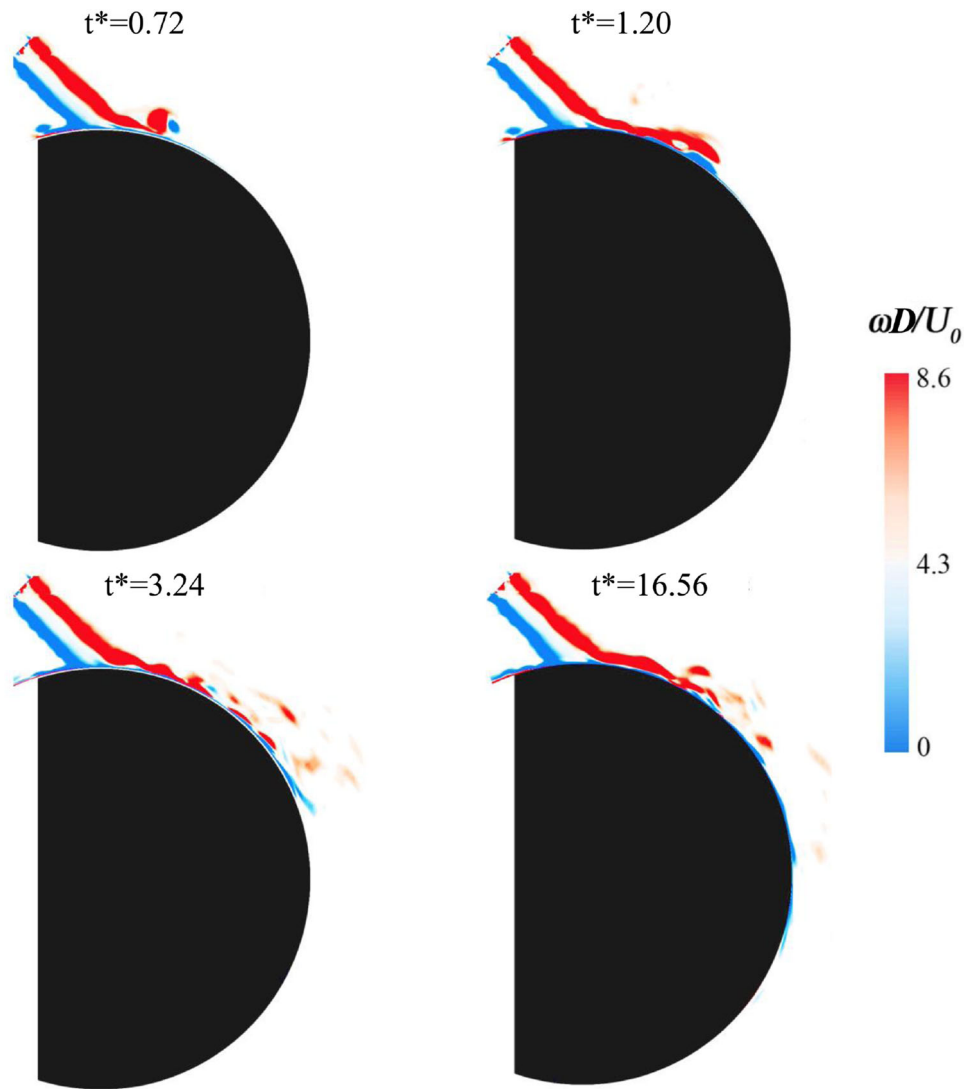
finding of a positive ring-like pressure band near the impingement region. The pressure band also changes sign repeatedly along the streamwise direction (positive–negative–positive–negative) until the pressure field becomes three-dimensional. The positive instantaneous wall pressure is located in the region of strong suction pressure in the time-averaged pressure field. The instantaneous pressure fields are strongly related to the vortex dynamics near the impinging region. This could be related to the secondary peak of heat transfer followed by the vortex-dipole formation.

Figure 6 illustrates the instantaneous vortex dynamics over time in the streamwise center plane (the same plane as the PIV measurement) across the impinging point. The vorticity magnitude is provided in a non-dimensional form. At  $t^* = 0.72$ , a mushroom-shaped vortex structure is formed by a pair of opposite-signed ring vortices. This behavior is called a vortex-dipole formation and was also observed by Cornaro et al. (1999) and New and Long (2015) in flow visualization experiments on laminar round jets impinging onto circular cylinders. The detachment of the vortex-dipole is observed where strong positive instantaneous wall pressure appears. The most notable feature is that the clockwise rotational vortex moves down to the wall when the counter-clockwise rotational vortex moves up from the surface, followed by a sign change of the instantaneous wall pressure, as shown at  $t^* = 1.2$ .

At  $t^* = 3.24$ , as the attached wall jet develops, a periodic generation of negative vortices can be observed very near the cylinder wall due to the no-slip condition. Strong positive vortices originating from the round jet edge are continuously elongated in the streamwise direction, but vortex-dipole and vortex separations periodically formed. The detached vortex-dipole moves away in the radial direction from the cylinder wall. Its vorticity rapidly decreases due to tilting and stretching. In steady state ( $t^* = 16.56$ ), a vortex-dipole formation occurs at approximately  $22^\circ$  from the flow symmetry plane, while vortex separation occurs further downstream at about  $47^\circ$ . Thereafter, the strong positive vortices are no longer observed, but the weakened vortex-dipole continues to move tangentially with the attached wall jet. Thin negative vortices are periodically generated very near the wall due to viscosity until the wall jet separates from the cylinder at approximately  $170^\circ$  from the flow symmetry plane.

### 3.2 Verification of the LES results with PIV measurements

Figure 7 shows the time-averaged velocity contours from when the flow reaches steady-state conditions. After the  $45^\circ$  oblique impingement of a round jet onto the cylinder surface, most of the fluid moves in one direction. At a Reynolds number of 11,800, the round jet impinges with a speed of 60 m/s and then quickly slows down further downstream. There is good agreement between the whole velocity fields obtained by LES and PIV, as shown in Fig. 7. The 3D curved wall jet develops along the curved surface after the impingement. Compared to normal impingement, the oblique impinging jet produces higher momentum and thickness of the curved wall jet. The wall jet is attached to the cylinder wall due to the Coanda effect, even though the velocity continuously decreases. The flow separation occurs around  $170^\circ$ – $180^\circ$  from the



**Fig. 6** Instantaneous vorticity contours developing on a circular cylinder

impinging point in the longitudinal direction at a Reynolds number of 11,800. The separation point is further downstream compared to those observed with a laminar round jet impingement onto a cylinder, which occur between  $85^\circ$  and  $115^\circ$  (New and Long 2015).

Figure 8 shows comparisons of the velocity profiles obtained at three different positions ( $\theta = 15^\circ$ ,  $60^\circ$ , and  $120^\circ$ ). The LES results show excellent agreement with the PIV results. Figure 8 shows that self-preserving wall jet profiles did not occur, because the wall jet could not fully develop due to flow separation. Significant variations of the mean velocity profiles near the wall region are observed in the flow direction. Compared to the results from a 2D curved wall jet, the maximum velocity point is higher from the wall. This can be explained by the lateral momentum flux in the case of the 3D curved wall jet, which is followed by a rapid decrease of the longitudinal momentum in the flow direction. As a result, flow separation occurs earlier than in the case of a 2D curved wall jet.



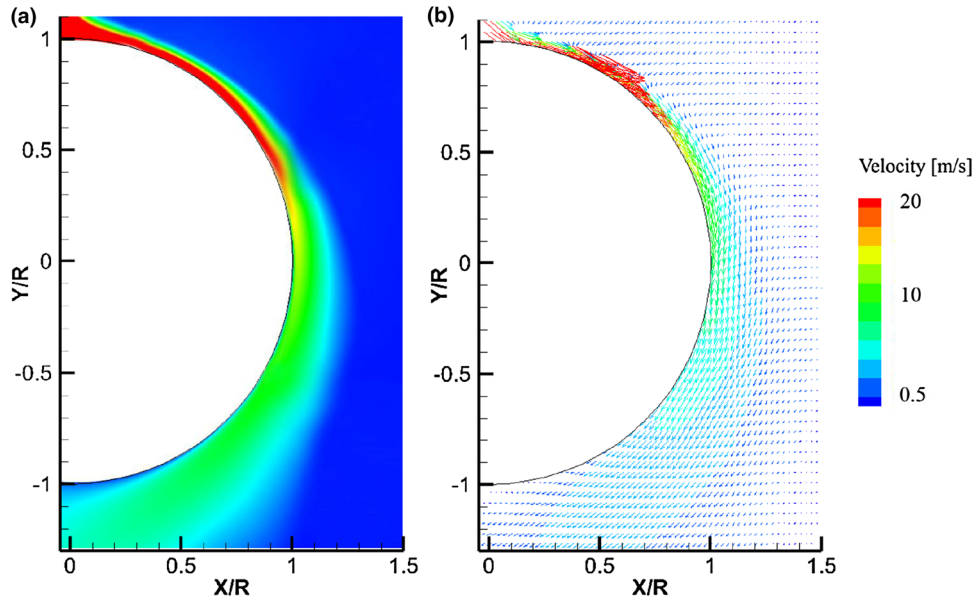


Fig. 7 Time-averaged velocity contours for a CFD and b PIV results

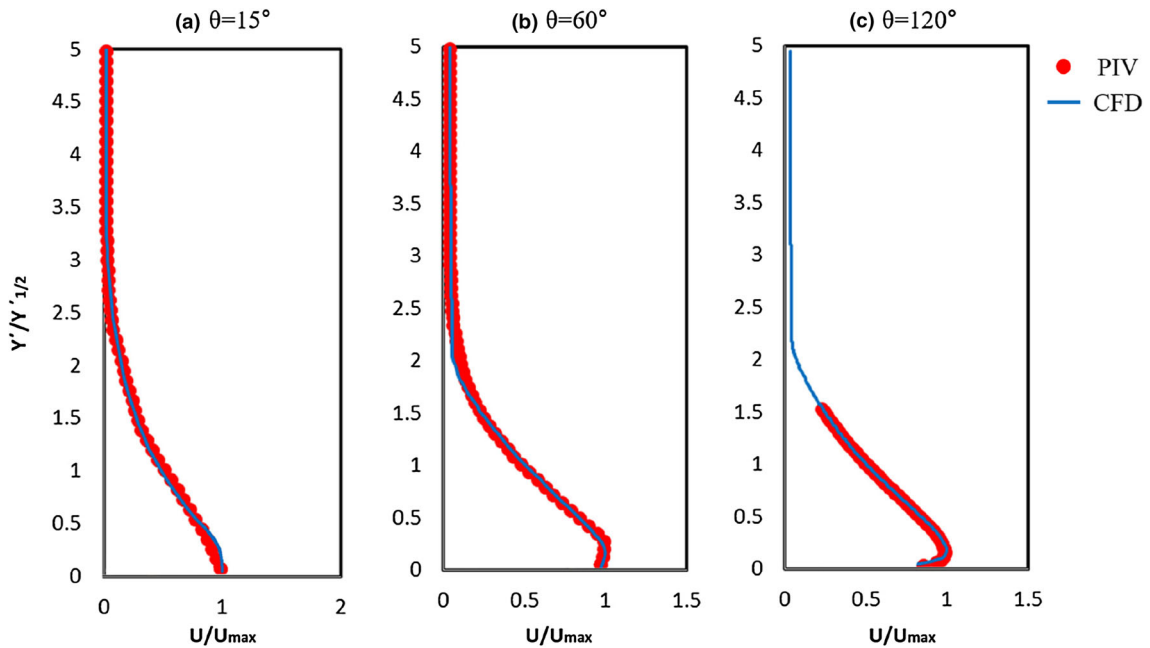


Fig. 8 Comparison of time-average velocity profiles in different positions (a, b, c) for both CFD and PIV results

### 4 Conclusions

The 3D flow characteristics of an oblique jet impinging onto a circular cylinder were visualized by the LES method, and the LES results were verified by a PIV experiment. The evolution of the vortex structures was examined in detail for when a turbulent round jet impinges onto a circular cylinder with inclination angle of  $45^\circ$  with a Reynolds number of 11,800. The distance from the nozzle exit to the cylinder surface was fixed at  $H/d = 4$ . After the impingement, the jet becomes a 3D curved wall jet and is attached to the cylinder wall far downstream due to the Coanda effect. The time-averaged pressure field indicated that the jet attachment is caused by strong suction pressure after the impingement. However, the instantaneous pressure field

revealed that positive and negative pressure bands appeared repeatedly with the 3D vortex structures near the impinging point.

Ring vortex structures appeared in only the initial stage after impingement ( $t^* < 1.0$ ). In the wall-jet development stage ( $1.0 < t^* < 10$ ), the attached jet moved rapidly in the streamwise direction rather than the spanwise direction. Small and strong positive vortices were observed near the cylinder wall, while bigger negative vortices were appeared in the upper region of the wall jet. These negative vortex structures seem to align with the streamwise direction.

When the 3D curved wall jet was fully developed ( $t^* > 15$ ), no further extension of the jet into the spanwise direction was observed. The spanwise extension of the jet was limited to  $\pm 1D$  from the impinging point. The clockwise rotational vortex moved down to the wall when the counter-clockwise rotational vortex moved up from the surface, followed by a sign change of the instantaneous wall pressure. The ensemble-averaged velocity fields obtained by LES and PIV shows good agreement.

**Acknowledgements** This work was supported by the National Research Foundation of Korea (NRF) grant funded by the Korea government (MSIP) (NRF-2016R1C1B2014255).

## References

- Ali ML, Ridoy R, Barua U, Alamgir MB (2016) Design and fabrication of a turbine flow meter. *J Mod Sci Technol* 4(1):16–26
- Brahma RK, Faruque O, Arora RC (1991) Experimental investigation of mean flow characteristics of slot jet impingement on a cylinder. *Wärme- und Stoffübertragung* 26:257–263
- Chan TL, Zhou Y, Liu MH, Leung CW (2003) Mean flow and turbulence measurements of the impingement wall jet on a semi-circular convex surface. *Exp Fluid* 34:140–149
- Cîrciu I, Boşcoianu M (2010) An analysis of the efficiency of Coanda-NOTAR anti-torque systems for small helicopters. *Incas Bull* 2:81–88
- Cornaro JC, Fleischer AS, Goldstein RJ (1999) Flow visualization of a round jet impinging on cylindrical surfaces. *Exp Thermal Fluid Sci* 20:66–78
- Danon R, Gregory JW, Greenblatt D (2016) Transient wall-jet flowing over a circular cylinder. *Exp Fluid* 57(141):1–14
- Didden N, Ho CM (1985) Unsteady separation in a boundary layer produced by an impinging jet. *J Fluid Mech* 160:235–256
- Donaldson CD, Snedeker RS (1971) A study of free jet impingement. Part I. Mean properties of free and impinging jets. *J Fluid Mech* 45(2):281–319
- Esirgemez E, Newby JW, Nott C, Ölçmen SM, Ötügen V (2007) Experimental study of a round jet impinging on a convex cylinder. *Meas Sci Technol* 18:1800–1810
- Fleischer AS, Kramer K, Goldstein RJ (2001) Dynamics of the vortex structure of a jet impinging on a convex surface. *Exp Thermal Fluid Sci* 24:169–175
- Han G, De Zhou M, Wygnanski I (2006) On streamwise vortices and their role in the development of a curved wall jet. *Phys Fluid* 18:1–14
- Jambunathan K, Lai E, Moss MA, Button BL (1992) A review of heat transfer data for single circular jet impingement. *Int J Heat Fluid Flow* 13:106–115
- Jeong J, Hussain F (1995) On the identification of a vortex. *J Fluid Mech* 285:69–94
- Keane RD, Adrian RJ (1992) Theory of cross-correlation analysis of PIV images. *Appl Sci Res* 49:191–215
- Kim M, Kim HD, Yeom E, Kim KC (2017) Flow characteristics of 3D curved wall jets on a cylinder. *J Fluid Eng.* <https://doi.org/10.1115/1.4038089>
- Kornblum Y, Goldstein RJ (1997) Jet impingement on semicylindrical concave and convex surfaces: part two-heat transfer. In: *International symposium on physics of heat transfer in boiling and condensation*, pp 597–602
- Landreth CC, Adrian RJ (1990) Impingement of a low Reynolds number turbulent circular jet onto a flat plate at normal incidence. *Exp Fluid* 9(1–2):74–84
- Lee DH, Chung YS, Kim DS (1997) Turbulent flow and heat transfer measurements on a curved surface with a fully developed round impinging jet. *Int J Heat Fluid Flow* 18:160–169
- Martin H (1977) Heat and mass transfer between impinging gas jets and solid surfaces. *Adv Heat Transf* 13:1–60
- Melling A (1997) Tracer particles and seeding for particle image velocimetry. *Meas Sci Technol* 8:1406–1416
- Neuendorf R, Wygnanski I (1999) On a turbulent wall jet flowing over a circular cylinder. *J Fluid Mech* 381:1–25
- Neuendorf R, Lourenco L, Wygnanski I (2004) On large streamwise structures in a wall jet flowing over a circular cylinder. *Phys Fluid* 16:2158–2169
- New TH, Long J (2015) Dynamics of laminar circular jet impingement on convex cylinders. *Phys Fluid* 27:024109
- Terzis A, Ott P, von Wolfersdorf J, Weigand B, Cochet M (2014) Detailed heat transfer distributions of narrow impingement channels for cast-in turbine airfoils. *J Turbomach* 136(9):091011
- Viskanta R (1993) Heat transfer to impinging isothermal gas and flame jets. *Exp Thermal Fluid Sci* 6:111–134
- Yi SJ, Kim M, Kim D, Kim HD, Kim KC (2016) Transient temperature field and heat transfer measurement of oblique jet impingement by thermographic phosphor. *Int J Heat Mass Transf* 102:691–702